JOURNAL OF NEUROTRAUMA 30:367–381 (March 1, 2013)

DOI: 10.1089/neu.2012.2339

Cellular Alterations in Human Traumatic Brain Injury: Changes in Mitochondrial Morphology Reflect Regional Levels of Injury Severity

Irina S. Balan,[1,2] Andrew J. Saladino,[3,7] Bizhan Aarabi,[5] Rudolf J. Castellani,[3] Christine Wade,[2] Deborah M. Stein,[2,4] Howard M. Eisenberg,[5] Hegang H. Chen,[6] and Gary Fiskum[1,2]

Abstract

Mitochondrial dysfunction may be central to the pathophysiology of traumatic brain injury (TBI) and often can be recognized cytologically by changes in mitochondrial ultrastructure. This study is the first to broadly characterize and quantify mitochondrial morphologic alterations in surgically resected human TBI tissues from three contiguous cortical injury zones. These zones were designated as injury center (Near), periphery (Far), and Penumbra. Tissues from 22 patients with TBI with varying degrees of damage and time intervals from TBI to surgical tissue collection within the first week post-injury were rapidly fixed in the surgical suite and processed for electron microscopy. A large number of mitochondrial structural patterns were identified and divided into four survival categories: normal, normal reactive, reactive degenerating, and end-stage degenerating profiles. A tissue sample acquired at 38 hours post-injury was selected for detailed mitochondrial quantification, because it best exhibited the wide variation in cellular and mitochondrial changes consistently noted in all the other cases. The distribution of mitochondrial morphologic phenotypes varied significantly between the three injury zones and when compared with control cortical tissue obtained from an epilepsy lobectomy. This study is unique in its comparative quantification of the mitochondrial ultrastructural alterations at progressive distances from the center of injury in surviving TBI patients and in relation to control human cortex. These quantitative observations may be useful in guiding the translation of mitochondrial-based neuroprotective interventions to clinical implementation.

Key words: cristae; electron microscopy; matrix; penumbra

Introduction

Animal models of traumatic brain injury (TBI) reveal that mitochondrial dysfunction is a critical factor in the cascade of events leading to apoptotic and necrotic neuronal cell death.[1–3] Being highly dynamic, the single mitochondrion represents only a transient manifestation of a constantly changing morphology. Mitochondrial morphology and intracellular distribution are dependent on numerous factors, including mitochondrial energy state, changes in membrane permeability, physical interactions with the cytoskeleton, mitochondrial dynamics (movement, fission, fusion), and the balance between mitochondrial biogenesis and degradation.[4–9]

Abnormalities in mitochondrial morphology accompany key events in the progression of excitotoxic neuronal injury[10] and are commonly observed in ischemic and traumatic brain injury (TBI) and in neurodegenerative disorders.[11–13] Patterns of mitochondrial ''morphodynamic'' changes may therefore be useful to monitor the alterations in the loss of cytoplasmic homeostasis and to provide insight into the subcellular pathophysiology of death.

Mitochondrial morphology, bioenergetics, and molecular pathways of apoptosis have been studied extensively in animal models of acute and chronic neurodegeneration. Despite the remarkable similarities of many of their pathophysiological alterations, a direct comparison between animals and humans may not always be possible. For example, numerous animal models of TBI have not fully replicated with exact fidelity the diversity of tissue damage and outcome characteristics of human TBI.[14,15] Taken together, therefore, accurate conclusions regarding the extent to which the mitochondrial dysfunction observed in animal TBI models resembles those in human TBI remains open to question. This work is presented in an effort to begin to bridge that gap.

[1]Department of Anesthesiology, [2]Center for Shock, Trauma, and Anesthesiology Research, [3]Department of Pathology, [4]Department of Surgery, Program in Trauma, [5]Department of Neurosurgery, [6]Division of Biostatistics and Bioinformatics, Department of Epidemiology and Public Health, University of Maryland School of Medicine, Baltimore, Maryland.
[7]Pathology Service, Veterans Affairs Medical Center, Baltimore, Maryland.

Direct determination of mitochondrial dysfunction after human TBI is limited by availability of tissue removed from living patients and rapidly processed to minimize *post-mortem* and *ex vivo* alterations.[16] Our study is the first to use rapidly fixed tissue removed from patients with TBI to qualitatively classify normal versus reactive and degenerative mitochondria by morphology, to quantitatively characterize mitochondrial ultrastructural changes after human TBI at progressive distances from the injury site, and to compare these data with control human cerebral tissue made available during the course of a lobectomy for the management of intractable epilepsy.

We hypothesize that the severity of closed head injury can be recognized by changes in cellular organelles, especially mitochondria, and that changes in two-dimensional (2D) mitochondrial structure (1) reflect overall severity of TBI, (2) reflect regional levels of brain injury severity, and (3) characteristically vary from one post-injury interval to another.

Methods

Clinical data

The relevant clinical details pertaining to our 22 patients with blunt traumatic brain injuries and one control patient (C-01) are listed in Table 1. Falls accounted for the largest group of patients (50%), followed by motor vehicle crashes (35%). The remaining 15% included two assault victims and one struck pedestrian. Our control patient #C-01 was a 30-year-old man who had medication-resistant partial onset seizures. Resected hippocampal tissue for therapeutic management showed neuronal loss and gliosis, as expected. The more remote temporal lobe tissue removed to gain hippocampal access was used in this study and was judged to be normal by light microscopy.

Patients with TBI varied widely with respect to age, Glasgow Coma Scores (GCS), and time intervals from TBI to surgical tissue collection and fixation. There were 18 males and 4 females. Computed tomography (CT) scan of the TBI patients included in our study revealed mixed density lesions of the cerebral cortical tissue that were characterized as focal contusions (low density) associated with intracerebral hematoma (high density). Extracerebral hematomas, such as acute subdural or acute epidural hematomas, were also present. These lesions were accompanied by intracranial hypertension and/or lateral shifts of cerebral hemispheres.

The patients with TBI underwent a resective surgery to prevent brainstem compression. Anesthesia was induced with fentanyl, propofol, and midazolam, followed by neuromuscular blockers, isoflurane, and fentanyl. The frontal lobe tissue only was resected in 80% of cases, the temporal lobe tissue only was resected in 10% of cases, and the cerebral cortical tissue of both frontal and temporal lobes was resected in 10% of cases. The average time from induction of anesthesia to tissue resection from TBI patients and from the one epilepsy lobectomy patient was 1 h and 2 h, respectively. Of TBI patients, 75% were discharged for rehabilitation (Rh); 20% of patients expired in hospital (EXP), and 1 of the 22 patients was discharged directly to home (HM). Standard preoperative management for all patients included mannitol and hypertonic saline. Other medications such as fentanyl, propofol, and morphine were used as necessary.

Program review and operative procedures

Brain tissues were removed during surgical debridement of the damaged cerebral cortex from patients admitted to the University of

Table 1. Brain Injury Study Patients' Clinical Data and Location of Submitted Tissue

Case #	*Post-injury interval (h)*	*GCS*	*Manner of injury*	*Sex*	*Age (years)*	*CT scan tissue density abnormality lobe/site location*	*Tissue resected from*	*Injury zone tissue*	*Patient discharged to*
C-01	n/a	15	SURG	M	30	Right amygdala & hippocampus	Temporal lobe	n/a	HM
1	5	10	FALL	F	72	Right temporal	Temporal lobe	N, F, P	Rh
2	6	3	MVC	M	23	Bifrontal, bitemporal, & biparietal	Frontal lobe	N, F	EXP
3	9	5	MVC	M	23	Right frontal and left temporal	Frontal lobe	N, F	EXP
4	12	14	FALL TOX	M	48	Left frontal, temporal, parietal, & occipital	Frontal lobe	N, F	Rh
5	13	3	FALL	M	50	Left frontal and midbrain	Frontal lobe	N, F	EXP
6	15	13	ASLT	M	73	Bifrontal, left temporal	Frontal lobe	N, F	Rh
7	16	9	FALL	M	32	Right frontal and temporal	Frontal lobe	N	Rh
8	23	14	FALL	F	68	Right frontal	Frontal lobe	N, F	Rh
9	27	4	MVC	M	26	Right frontal, temporal, & parietal	Frontal & temporal lobes	N, F	Rh
10	32	13	FALL	M	48	Bifrontal, left temporal	Frontal & temporal lobes	N, F	Rh
11	38	13	MVC	F	16	Right frontal	Frontal lobe	N, F	Rh
12	38	15	MVC	M	27	Bifrontal	Frontal lobe	N, F, P	HM
13	39	11	MVC	M	45	Bifrontal	Frontal lobe	N, F	Rh
14	65	6	ASLT	M	76	Right frontal, temporal, & parietal	Frontal lobe	N, F, P	Rh
15	68	14	FALL	M	74	Right frontal	Frontal lobe	N, F	EXP
16	71	14	MVC	M	15	Left frontal	Frontal lobe	N, F	Rh
17	72	15	FALL	M	30	Bifrontal, left temporal	Frontal lobe	N, F	Rh
18	84	3	MVC	M	23	Bifrontal, right temporal, & parietal	Frontal lobe	N, F	Rh
19	109	3	FALL TOX	M	38	Bifrontal	Frontal lobe	N, F	Rh
20	136	7	PED	M	45	Bitemporal	Temporal lobe	N, F	Rh
21	171	8	FALL	M	51	Left frontal, temporal, & parietal	Frontal lobe	N, F	Rh
22	175	14	FALL	F	78	Right parietal	Parietal lobe	N, F	Rh

GCS, Glasgow Coma Scale; CT, computed tomography; SURG, surgical resection only; n/a, not applicable; HM, home; FALL, fall; N, Near; F, Far; P, Penumbra; Rh, rehabilitation; MVC, motor vehicle crash; Exp, expired; TOX, intoxicated; ASLT, assault; PED, pedestrian struck.

Maryland School of Medicine R. Adams Cowley Shock Trauma Center with a clinical diagnosis of blunt TBI and from one patient who underwent an epilepsy lobectomy at the Baltimore Veterans Affairs (VA) Medical Center. All neurosurgical procedures and tissue studies were approved by both the University of Maryland Baltimore Institutional Review Board and the VA Maryland Health Care System Research and Development Committee. Their decision was that informed consent was not required for this project.

The resected cortical tissues in all 22 TBI patients were classified visually by the same neurosurgeon as to level of degenerative changes based on tissue texture, coloration, and presence of microhemorrhage. These areas were designated as Near (zone of most advanced tissue damage), and Far (less damaged adjacent tissue). In three cases, a separate fragment of involved tissue was also removed that appeared near-normal (Penumbra). The majority of specimens were from focal cerebral contusions or mixed density lesions by CT.

Fixation and electron microscopic procedures

Cortical fragments, approximately 10 to 15 mm in greatest dimension, were fixed in 4% paraformaldehyde-0.1 M phosphate buffer (pH 7.4) in the surgical suite within 10 min of separation from the patient's vascular circulation and kept at 4°C until a secondary fixation was performed using a mixture of 4% paraformaldehyde and 1% glutaraldehyde with 0.1 M phosphate buffer pH 7.4 (4F1G) for 48 hours at 4°C.[17] Before 4F1G fixation, the tissues were divided into smaller $\sim$1 mm fragments. These fragments were then rinsed in 0.1 M sodium cacodylate containing 0.2 M sucrose for 10 min and post-fixed in 1% osmium tetroxide-0.1 M phosphate buffer, pH 7.4, for 1 h at 4°C. Subsequently, they were *en bloc* stained with uranyl acetate for 1 h, dehydrated in increasing concentrations of ethanol, infiltrated with solutions containing different proportions of propylene oxide and Poly/Bed-812 embedding medium and embedded in Poly/Bed-812 medium.

To facilitate orientation during the electron microscopy study, $\sim$1 μm semi-thin sections were stained with toluidine blue and examined with a Nikon E800 microscope equipped with an Optronics color digital camera. Ultrathin sections (100 nm), obtained with a Porter-Blum ultramicrotome, were stained with uranyl acetate and lead citrate and observed in a Tecnai G2 transmission electron microscope (TEM) equipped with AMT V600 software.

Morphometric and statistical analysis

A minimum of 30 TEM images were evaluated for each injury zone of each of the 22 TBI patients and for the control patient presented in Table 1. Mitochondrial profiles appearing in these images were classified according to the following structural criteria: (1) 2D shape; (2) outer membrane integrity: preserved versus disrupted; (3) inner membrane integrity: preserved versus disrupted; (4) cristate alignment: orthodox/parallel versus random; (5) cristate membrane integrity: preserved versus disrupted; (6) intracristate space: parallel versus open; (7) matrix density: condensed, moderate, clear; (8) dense matrix inclusions: absent versus present. For our representative case, patient #12, we also quantified mitochondrial mitophagy, fission, fusion, outer membrane ''budding,'' and mitochondria that showed bizarre presentations of their 2D shapes and internal structure.

Statistical comparisons of the number of different mitochondrial profiles present in the three injury zones were performed using tissue from TBI case #12 for two primary reasons: (1) This patient was one of only three in our series in whom all three progressive injury zones were identified and separated by the neurosurgeon; (2) tissue from this patient was obtained at an intermediate post-injury time of 38 h and exhibited the full range of normal and abnormal mitochondrial 2D profiles observed in all other patients in our series.

TBI patient #12 was a 27-year-old man who sustained blunt head trauma with a brief loss of consciousness at the scene of a motor vehicle accident. He was found to have multiple facial fractures, pneumocephalus bifrontal contusions, and subarachnoid hemorrhage. His GCS score on admission was 15, and neurosurgery with tissue collection and fixation was conducted 38 h post-injury. At the time of surgery, his GCS was 14. He recovered well post-surgery and was discharged to home 5 days after admission (Table 1).

For morphometric analysis of mitochondria, 4400$\times$ magnification 8-bit gray scale TEM images for each Near ($n=30$), Far ($n=32$), Penumbra ($n=50$) zones of patient #12 and from control tissue obtained from one epilepsy lobectomy patient ($n=36$) were simultaneously and randomly selected using AMT V600 software. The brightness of the beam, gain/contrast options, and exposure time were normalized electronically. MetaMorph software was used to count the number of different mitochondrial morphological profiles present on each image (actual image size is 44 μm^2) and to measure the optical absorbance of each mitochondrion present on the images. Mitochondria were counted in the neuronal processes in all three injury zones and control cortex, and in neuronal perikarya of Far and Penumbra zones and control tissue.

The neuronal cell bodies and their processes were distinguished from glial cell bodies and their processes using previously described morphologic criteria.[18–22] Typically, neurons have a large, round nucleus containing a conspicuous, large, spherical nucleolus, and are located in the center of the cell body. The karyoplasm lacks chromatin particles and shows typically clear vesicular appearance. Neuronal cells are recognized by the presence of numerous free polysomes and Nissl bodies. Axons consist of thin processes interspersed with boutons containing synaptic vesicles. Axons may be myelinated or unmyelinated. Axons and dendrites contain neurofilaments and microtubules, where they form parallel array. Dendrites are characterized by synapses, both asymmetric, recognized by thickened postsynaptic densities, and symmetric, recognized by pleomorphic vesicles and uniform thinner densities on pre- and postsynaptic sides. Spiny dendrites are sub-divided into shafts and spines connected to their dendritic shafts through necks.

The optical absorbance of each outlined mitochondrion was calculated as previously described.[23] Using the MetaMorph program, we measured average intensities of the outlined mitochondria at white light that correspond to intensity amplitudes of all pixels in the object divided by area. The absorbance of each outlined mitochondrion was calculated by subtracting the measured intensity amplitude (I) from maximum pixel intensity amplitude (Imax) in brain slice images.

Absorbance = Imax – I
Imax = 255 (pixel values are from 0 to 255)
I = measured pixel intensity amplitude

In addition, we measured the average absorbance values of the cytosolic areas outlined around mitochondria for each image. These values were then subtracted from the absorbance values of mitochondria.

The statistical differences for pairwise comparisons of number of different mitochondrial morphological profiles present on each TEM image between three injury zones and control tissue were determined by Wilcoxon rank sum test. Statistical analyses were performed using SAS version 9.2 statistics software. The data are presented as mean $\pm$ standard error.

Results

Range of mitochondrial architectural profiles

Based on published ultrastructural studies on isolated mitochondria, mitochondria in tissue culture and tissue slices, and mitochondria observed in perfusion-fixed primate brains,[24–31] the human cortical mitochondrial structural patterns identified in our study of the 23 human cases were divided into four categories: normal, normal reactive, reactive degenerating, and end-stage degenerating profiles. Normal profiles are characterized by a

moderately dense matrix and a normal cristate architecture (Figs. 1A, B, C). This profile is often referred to as the ''orthodox conformation.''[26,32] Normal reactive profiles exhibit a tightly condensed matrix and widely expanded intracristate space (Fig. 1D), indicative of a ''condensed conformation.''[26,32]

Some mitochondria exhibit condensed twisted matrix (Fig. 1E). This category also includes mitochondria with unusual shapes such as tubular loops (Fig. 1F) and tubular donut-shaped mitochondria (Fig. 1G). Because we have analyzed 2D TEM slices, we cannot exclude that these 2D shapes are results of the slicing plane rather than anomalous mitochondrial fusion.[6] Reactive/degenerating profiles include ''thread-grain-transitions,''[33] which are characterized by segmented mitochondria that vary from low to high amplitude swollen profiles. The matrix within these mitochondria may be normal to electron lucent but maintain semblance of original cristate architecture (Fig. 1H, L). This category also includes mitochondria undergoing membrane blebbing and ''budding'' (Fig. 1I, J), and dividing mitochondria with partial loss of cristae and often granular matrix (Fig. 1J). The buds either resemble tiny mitochondria (Fig. 1J), or they contain a core of homogeneous material and resemble small mitochondria-derived vesicles (Fig. 1M).[34]

Also present are round, symmetrical mitochondria with clear matrix (Fig. 1K). While small spherical structures could represent filamentous mitochondria cut orthogonally, they are not accompanied by the presence of filamentous or small ellipsoidal mitochondria within the same image, as would be expected from orthogonally cuts of asymmetric mitochondria.

End-stage degenerating mitochondria are typified by spherical fission products, some showing high amplitude swelling (Fig. 2A) and swollen collapsing mitochondria (Fig. 2B). Inner membrane-associated dense granular inclusions are also present in this category and are a hallmark of mitochondrial calcium overload and irreversibly injured mitochondria (Fig 2C).[35,36] Many mitochondria exhibit dark diffusely granular matrix (Fig. 2D). Some of end-stage degenerating mitochondria are enveloped by residual membranes of autophagic vacuoles (mitophagy) (Fig. 2E).[37]

Mitochondrial accumulation is evident in bulbous enlargements of neuronal processes and was frequently observed within the Far zone (Fig 3A, B). Massive mitochondrial accumulation is most evident in tissue obtained near the end of the first week post-injury (Fig. 3B). These mitochondria exhibit characteristics present in all four survival profiles.

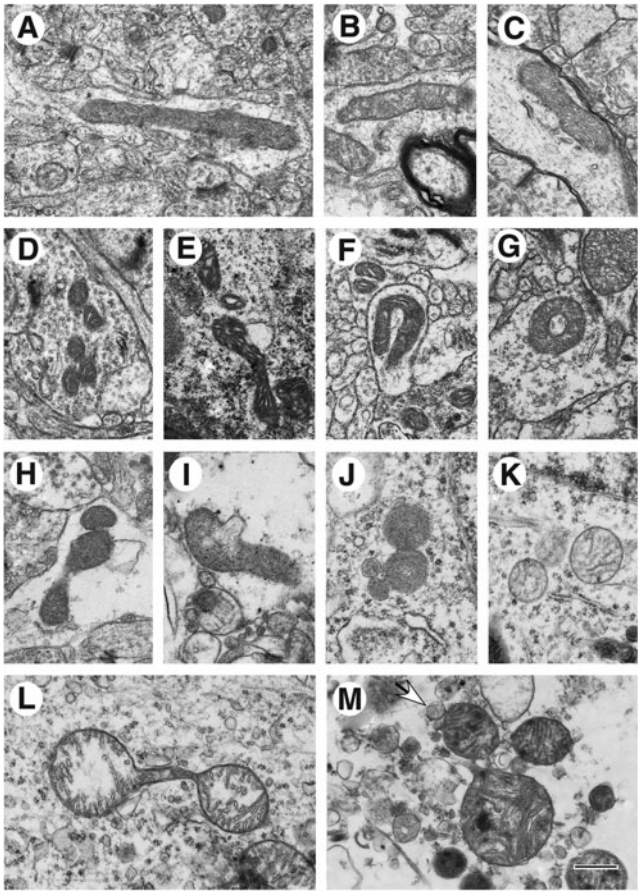

FIG. 1. Human brain mitochondrial ultrastructural patterns. (**A–C**) Normal survival category (A, Case #12, Penumbra zone; B, Case #1, Far zone; C, Case #1, Penumbra zone); (**D–G**) Normal reactive category (D, Case #12, Far zone; E, Case #13, Far zone; F, Case#11, Far zone; G, Case #1, Penumbra zone); (**H–M**) Reactive/degenerating category (H, Case #13, Far zone; I, Case #12, Far zone; J, Case #16, Far zone; K, Case #14, Penumbra zone; L, Case #17, Far zone; M, Case #2, Near zone; arrow shows mitochondria-derived vesicles). Scale bar equals 500 nm.

Progression of structural changes in different zones of injury and comparison with control

In the 22 TBI cases studied, similar mitochondrial structural patterns were observed consistently from one injury zone to the next within each of three post-injury intervals defined as ''early'' (less than 1 day post-injury), ''intermediate'' (between 1 and 3 days post-injury), and ''late'' (approximately 3 days post-injury and later). Within the early injury interval, the central or Near zone of injury exhibits predominantly reactive/degenerative and end-stage degenerative changes in mitochondrial morphology (Fig. 4A). The more peripheral Far zone and Penumbra exhibit primarily normal and normal reactive mitochondrial morphotypes (Fig. 4B, C). Some mitochondria in these two zones are reactive/degenerative, exhibiting primarily thread-grain-transition profiles (Fig. 4D). In parallel, parenchymal cells in these two zones display better preservation than that observed in the Near zone.

Slight cytoplasmic, axonal, and dendritic swellings are noticeable in the Far zone and Penumbra. In the Near zone of injury, there is moderate to severe swelling of parenchymal cells and processes. When the GCS score is low (GCS = 3–5; Cases #2, 3, and 5; Table 1), total disruption of tissue architecture and presence of primarily end-stage degenerating mitochondria are characteristic for all injury zones (Fig. 5A, B).

Within the intermediate post-injury interval, cellular edematous changes are maximal with a peak at approximately 36–42 hours post-injury. The widest variations in mitochondrial pathological changes among different injury zones are present within this injury interval. Penumbra and Far zone exhibit all four mitochondrial profile categories, but they differ quantitatively between these two zones. The Near zone of injury contains primarily reactive/degenerating and end-stage degenerating mitochondria.

Within the late post-injury phase, normal-appearing mitochondria are infrequent even within the Penumbra zone. Reactive/degenerating mitochondria are abundant, however, in both the Penumbra and Far zones (Fig. 6A–C). The Near zone contains primarily end-stage degenerating mitochondria (Fig. 6D).

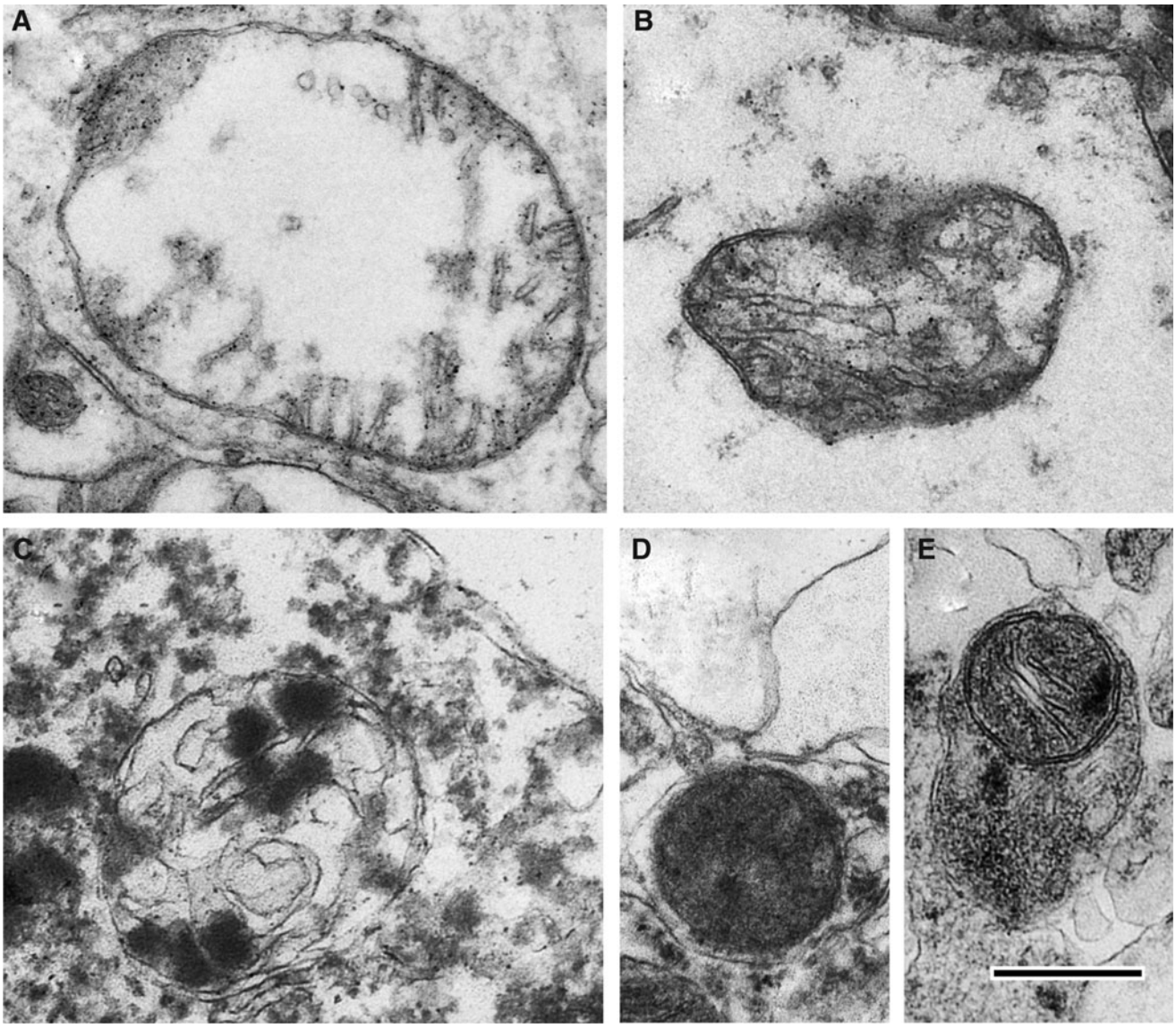

FIG. 2. End-stage degenerating mitochondrial profiles. (**A**) Case #12, Far zone. High amplitude swollen mitochondrion with electron-lucent matrix. (**B**) Case# 13, Far zone. Swollen collapsing mitochondrion. (**C**) Case #10, Near zone. Swollen mitochondrion with matrical dense inclusions. (**D**) Case #22, Near zone. Mitochondrion with dark diffusely granular matrix. (**E**) Case #7, Near zone. Spherical mitochondrion with segmental area loss of cristate structure and matrical densities is enveloped by double membranous authophagic vacuole (mitophagy). Scale bar equals 500 nm.

The majority of mitochondrial profiles present in control cerebral cortex are normal and normal reactive, as expected. Normal tubular mitochondria are present almost exclusively in neuronal processes (Figs. 7A–C). In contrast, mitochondria of neuronal cell bodies are predominantly ovoid or rounded (Figs. 8A–C). While normal cristate architecture is maintained in most mitochondria, few exhibit disrupted cristae or an apparent loss of matrix material (Fig. 8C). A few reactive/degenerating and end-stage degenerating mitochondrial profiles are also apparent in the control tissue sample (Figs. 7B,C, 8C).

Histologic comparisons between cerebral cortex from TBI and control (epilepsy lobectomy)

Control cerebral cortex obtained during the course of an epilepsy lobectomy (Fig. 9A) displays medium-size pyramidal neurons and glial cells scattered in a field of predominantly unmyelinated axons, consistent with cortical levels 4, 5, and 6 (Fig. 9A). In contrast to TBI brain tissue, no evidence for edema is present, and neuronal nuclei are fully rounded, containing stippled, homogeneously distributed chromatin and prominent nucleoli. Neuronal cytoplasmic swelling is barely noticeable. Vascular stasis is widespread, but perivascular hemorrhage is minimal to absent.

Characteristic histologic changes that readily distinguish each of the three injury zones present in tissue resected from Patient #12 are evident by examination using light microscopy (Figs. 9B–D). In the Penumbra zone of injury, vascular stasis is focal and mild, whereas perivascular hemorrhage is not evident. Neurons are recognizable by their large size and fully rounded nuclei, which exhibit evenly dispersed stippled chromatin (Fig. 9B). Many nuclei contain prominent intact nucleoli. Focally, there is mild to moderate intracellular swelling restricted primarily to perineuronal areas (Fig. 9B).

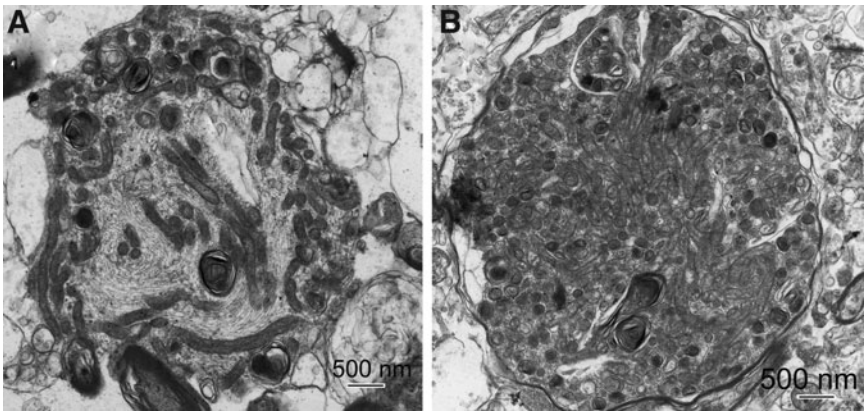

FIG. 3. Accumulation of mitochondria in bulbous enlargements of neuronal processes present in injured cortex, Far zone. (**A**) Case #12, Far zone. Disorientation of microtubules and mitochondria are predominantly accumulated in the periphery of the process enlargement. (**B**) Case #21, Far zone. Tightly packed mitochondria in a process enlargement.

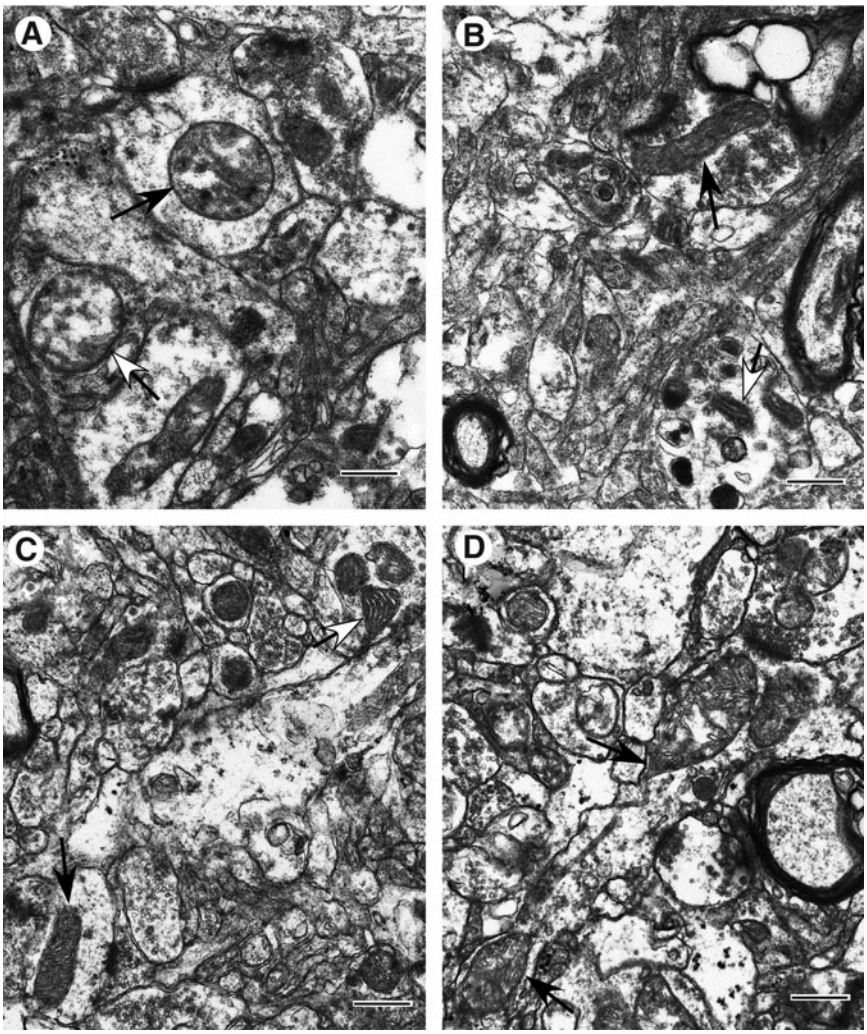

FIG. 4. Ultrastructural pathology of injured cortex at early injury phase (less than 1 day post-injury; Case #1). (**A**) Near zone. Neuropil with frequent swollen processes showing high amplitude swollen mitochondria (arrows). Inner membrane-associated dense granular inclusions are present in a mitochondrion (black arrow). (**B**) Far zone. Slight to moderate cytoplasmic swellings are noticeable. Mitochondria are primarily normal (black arrow) and normal reactive (white-head arrow). (**C**) Penumbra zone. Slight to moderate cytoplasmic swelling. Mitochondria are predominantly normal orthodox (black arrow) or normal reactive (white head arrow). (**D**) Far zone. Neuropil with swollen processes showing mitochondrial changes. Note the teardrop-shaped mitochondrial profiles with thin thread-like extension (arrows) suggestive of a thread-grain transition. Scale bars equal 500 nm.

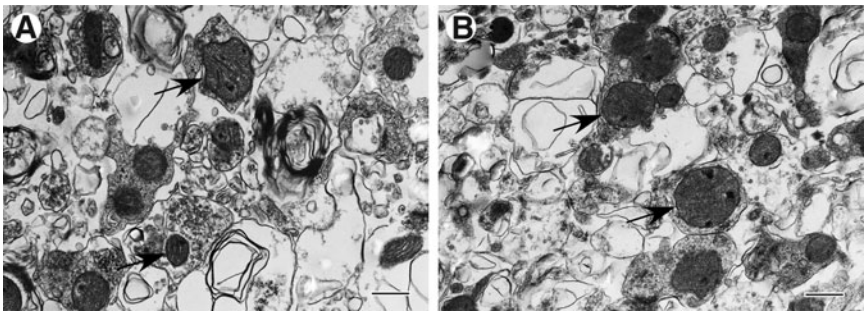

FIG. 5. Ultrastructural pathology of injured cortex at early injury phase (less than 1 day post-injury; Case #2). (**A**) Far zone. (**B**) Near zone. A and B: Total disruption of tissue architecture and end-stage degenerating mitochondria (arrows) present. Scale bars equal 500 nm.

In the Far zone of injury, survey sections (Fig. 9C) are variable in appearance, but parenchymal cells display better preservation than that observed in the Near zone (Fig. 9D). Patchy vascular stasis, perivascular hemorrhage, and slight to moderate focal cytoplasmic and axonal swelling are also noticeable in the Far zone. As with the Penumbra, neurons are easily recognized by their size, shape, and distinctive nuclei; however, many neuronal nuclei in the Far zone exhibit irregularly aggregated chromatin. Focally, there is moderate to severe swelling restricted to the perineuronal area, with the involved perikarya presenting a reciprocal decrease in the cross-sectional area of their cytoplasm.

In Near zone of injury (Fig. 9D), total disruption of tissue architecture is obvious, characterized by edematous loose

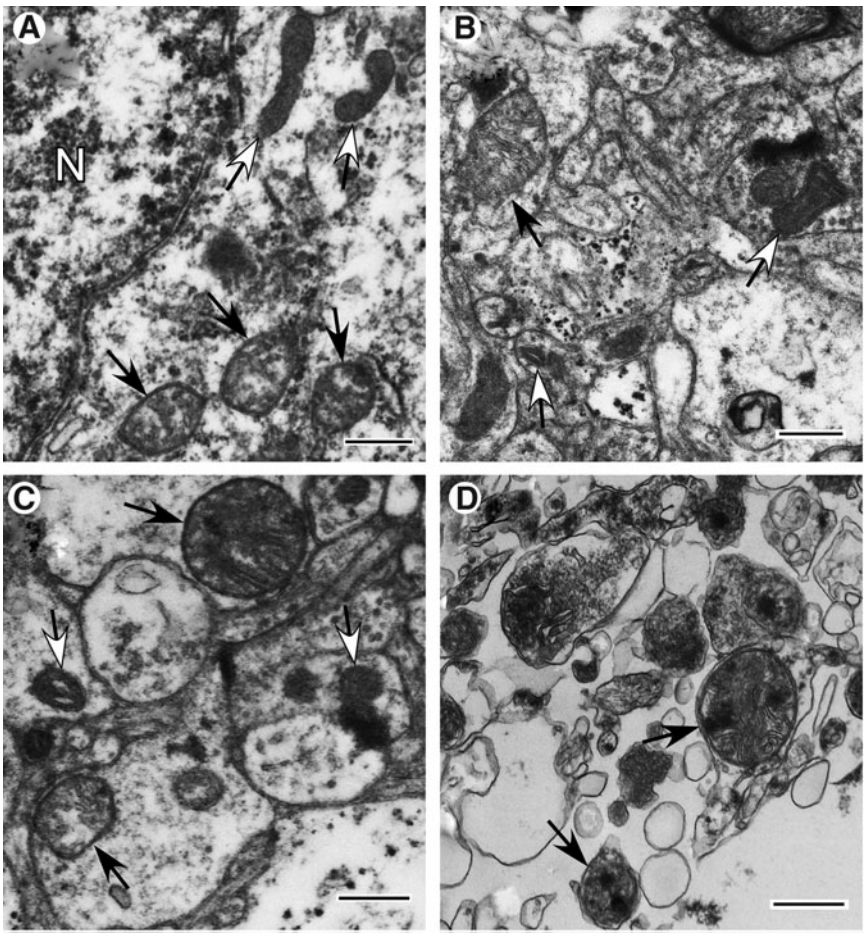

FIG. 6. Ultrastructural pathology of injured cortex at late injury phase (approximately 3 days post-injury and later; Case #14). (**A,B**) Penumbra zone. (**C**) Far zone. (**D**) Near zone. (A) Neuronal cell body showing a group of mitochondria that exhibit abnormally spherical profiles with clear matrix space and disruption of cristate architecture (black arrows). Another group of mitochondria exhibit normal reactive structure (white-head arrows). N-nucleus. (B) Area of neuropil with slight to moderate swelling of neuronal processes. Mitochondria exhibit normal reactive (white-head arrows) and reactive/degenerating (black arrow) profiles. (C) Neuropil with frequent swollen processes showing normal reactive (white-head arrows) and reactive/degenerating (black arrows) mitochondrial changes. (D) Total disruption of tissue architecture and end-stage degenerating mitochondria (arrows) present. Scale bars equal 500 nm.

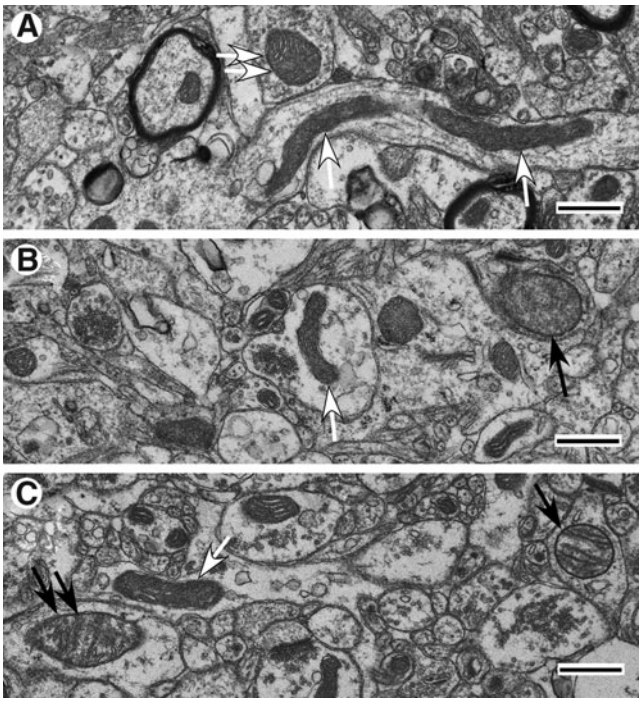

FIG. 7. Mitochondrial profiles present in neuropil in normal cortex obtained by temporal lobectomy. (**A**) Neuronal process contains long orthodox mitochondria (arrows) in close association with microtubules. A spherical mitochondrion (double arrows) with slightly condensed matrix is present in an adjacent cell process. (**B**) Mitochondria are predominantly tubular in shape (white arrow), their matrix density is moderately condensed, and cristate architecture is well preserved. A rare large spherical mitochondrial profile (black arrow) is contained within another cell process. (**C**) Predominantly tubular mitochondria (white arrow) with moderately condensed matrices are present. Occasionally, cristae are parallel to the mitochondrial long axis (black arrow). A mitochondrion shows moderate rounding and fusiform shape change of a late thread-grain transition (double black arrows). All scale bars equal 500 nm.

necrotic material, marked dilatation of vascular spaces, red blood cell congestion, stasis, and focal areas of interstitial hemorrhage.

Quantitative ultrastructural characteristics of mitochondria present in injured cerebral cortex

The Near zone exhibits marked parenchymal degenerative changes and is characterized by massive cytoplasmic swelling, rupture of plasmalemmal and nuclear membranes with surface bleb and vesicle formation, and disintegration and loss of cytoplasmic organelles (Figs.10A–D). The neuropil displays marked interstitial edema and swollen cell processes (Figs. 10C,D). Virtually all discernible mitochondria fall within the classifications of either reactive/degenerating ($37.4\% \pm 5.3$) (Fig. 1 H-M) or end-stage degenerating ($62.6\% \pm 5.3$) (Figs. 2A–E) (Fig. 11). Subsets of these mitochondria include those with matrical dense granular inclusions ($26.4\% \pm 4.5$) (Fig. 2C) and those with dark diffusely granular matrix ($28.8\% \pm 4.8$) (Fig. 2D).

The Far zone presents evidence of mild to moderate focal intra- and extracellular edema (Figs. 12A–C). All four survival mitochondrial categories are noticeable in this zone, with the normal orthodox profile (Figs. 1A-C) being relatively scarce ($1.6\% \pm 0.8$) (Fig. 11). Normal reactive mitochondria are prevalent ($63.3\% \pm 3.9$), and include mitochondria with condensed matrix or dense twisted matrix (Figs. 1D, E; 12B, C). Among reactive/degenerating mitochondria, there are teardrop-shaped mitochondrial profiles interconnected with thin thread-like structures (Figs. 1L; 12A), suggestive of mitochondrial thread-grain transition.[33] This zone exhibits significantly less end-stage degenerating mitochondria ($27.2\% \pm 3.5$) ($p \leq 0.0001$) than those present in the Near zone (Fig. 11). The Far zone also displays significantly fewer end-stage degenerating mitochondria with matrical dense granular inclusions ($2.8\% \pm 1.1$ vs. $26.4\% \pm 4.5$) (Fig. 2C) and with dark diffusely granular matrix ($14.5\% \pm 2.6$ vs. $28.8\% \pm 4.8$) (Fig. 2D) than Near zone ($p \leq 0.05$ and $p \leq 0.0001$, respectively).

The Penumbra zone appears far more normal than both the Near and Far zones: however, morphologically altered mitochondrial profiles are present in both neuronal cell bodies and processes (Figs. 13A–D). The Penumbra zone exhibits all four mitochondrial

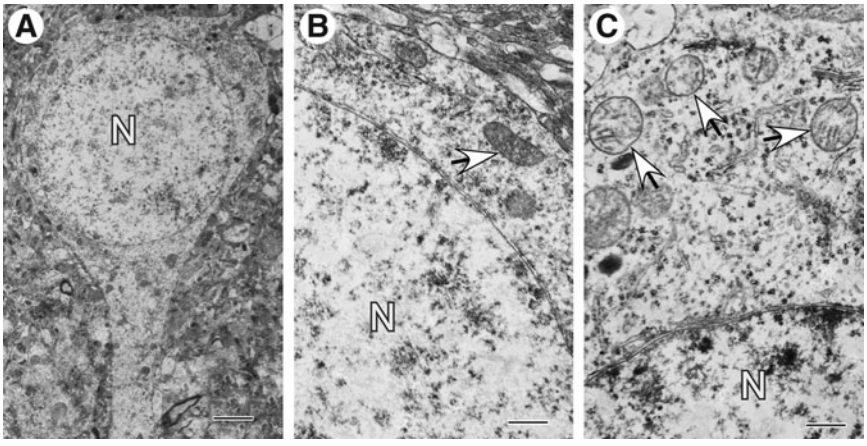

FIG. 8. Mitochondrial profiles present in neuronal cell bodies in normal cortex obtained by temporal lobectomy. (**A**) Pyramidal neuron with good preservation of nucleus (N), cytoplasm, and even distribution of organelles. (**B**) Fragment of neuronal cell body with well-preserved normal mitochondria (arrow). (**C**) Fragment of neuronal cell body showing spherical mitochondria with clear matrix space and disruption of cristate architecture (arrows). Scale bars equal A: 2 μm; B and C: 500 nm.

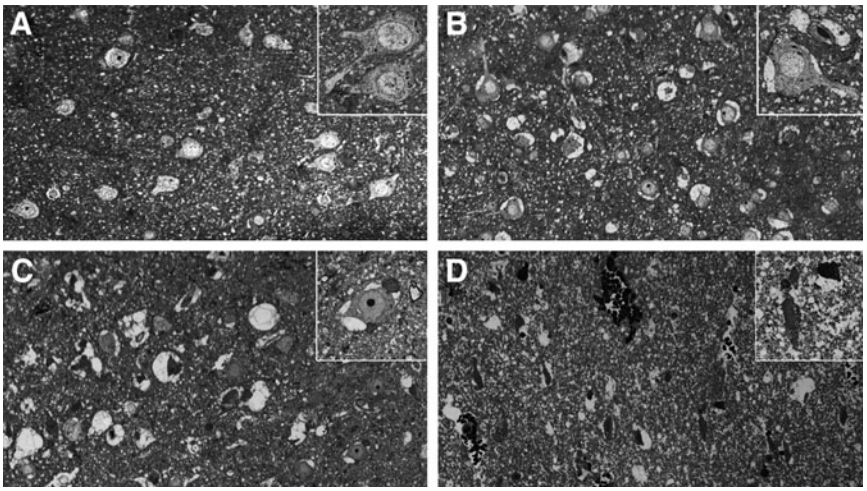

FIG. 9. Toluidine blue stained semi-thin sections of human brain. (**A**) control cortical tissue; (**B–D**) Case #12 (B, injured Penumbra zone; C, injured Far zone; D, injured Near zone). A–D: original magnification × 200; insertions within A–D: original magnification × 550.

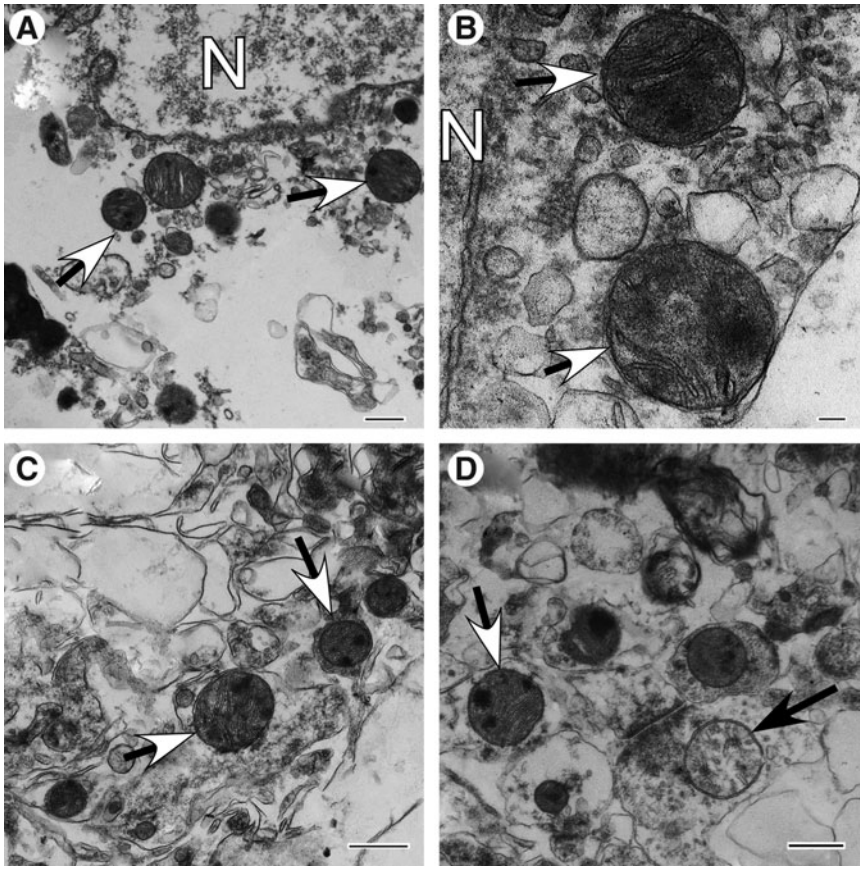

FIG. 10. Ultrastructural pathology of injured cortex, Near zone (Case #12) at intermediate injury phase (between 1 and 3 days post-injury). (**A**) Enlarged area of ruptured cell shows advanced cytoplasmic dilution and spherical mitochondria containing multiple matrix densities and dark diffusely granulated matrix (arrows). N, nucleus. (**B**) High magnification of perinuclear area. Mitochondria show segmental area loss of cristate structure and soft matrical densities (arrows). N, nucleus. (**C**) Enlarged area of neuropil shows interstitial edema, swollen processes, cytoplasmic fragmentation, and spherical mitochondria containing multiple matrix densities in a dark diffusely granulated matrix (arrows). (**D**) Area of advanced cellular disruption. Mitochondria show both retention of matrix with large hard densities or soft semicrystalline densities (arrow with white head) and matrical swelling and clearing (black arrow). Scale bars for A, C, and D equal 500 nm; for B, 100 nm.

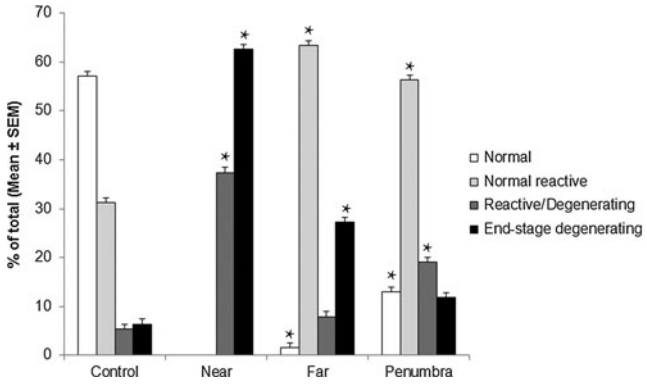

FIG. 11. Distribution of cerebral cortex mitochondria among morphologic categories. Categories were defined as normal, normal reactive, reactive/degenerating, and end-stage degenerating. Distributions among these categories are given for control tissue and TBI tissue separated into Near, Far, and Penumbra injury zones. Measurements were made within 2D fields (44 μm^2) of ultrathin sections (100 nm). The number of fields used for control, Near, Far, and Penumbra were 36, 30, 32, and 50, respectively. Total mitochondrial number counted for Control, Near, Far, and Penumbra were 712, 346, 378, and 621, respectively. Values represent the means ± standard error (SEM). *$p \leq 0.0001$ when compared with control.

morphology categories, as seen in the Far zone, but the number of normal orthodox mitochondria (Fig. 1A-C; 13B) in Penumbra (12.9% ± 2.0) is higher ($p \leq 0.0001$) than in Far zone (Fig. 11). The optical absorbance of orthodox mitochondria in these two TBI zones is less than that measured in control tissue ($p \leq 0.001$) (Fig. 14). This finding suggests that the matrix of the orthodox mitochondria in the TBI tissue may have been more edematous because of osmotic swelling.[38]

The Far and Penumbra injury zones exhibit statistically equivalent numbers of normal reactive mitochondria (Figs. 1D–G); however, the number of end-stage degenerating mitochondria (Figs. 2A, B, D, E) in the Penumbra zone is significantly less ($p \leq 0.0001$) than in the Far zone (Fig. 11). The Penumbra zone displays significantly fewer mitochondria with dark diffusely granular matrix (Fig. 2D) (7.1% ± 1.3) than present in the Far zone ($p \leq 0.05$). There are no mitochondria with matrical dense inclusions detectable in the Penumbra zone (Fig. 2C). The Penumbra zone exhibits significantly fewer normal "orthodox" mitochondria (12.9% ± 2.0 vs. 57% ± 3.1) ($p \leq 0.0001$) and a significantly larger number of reactive/degenerating mitochondria

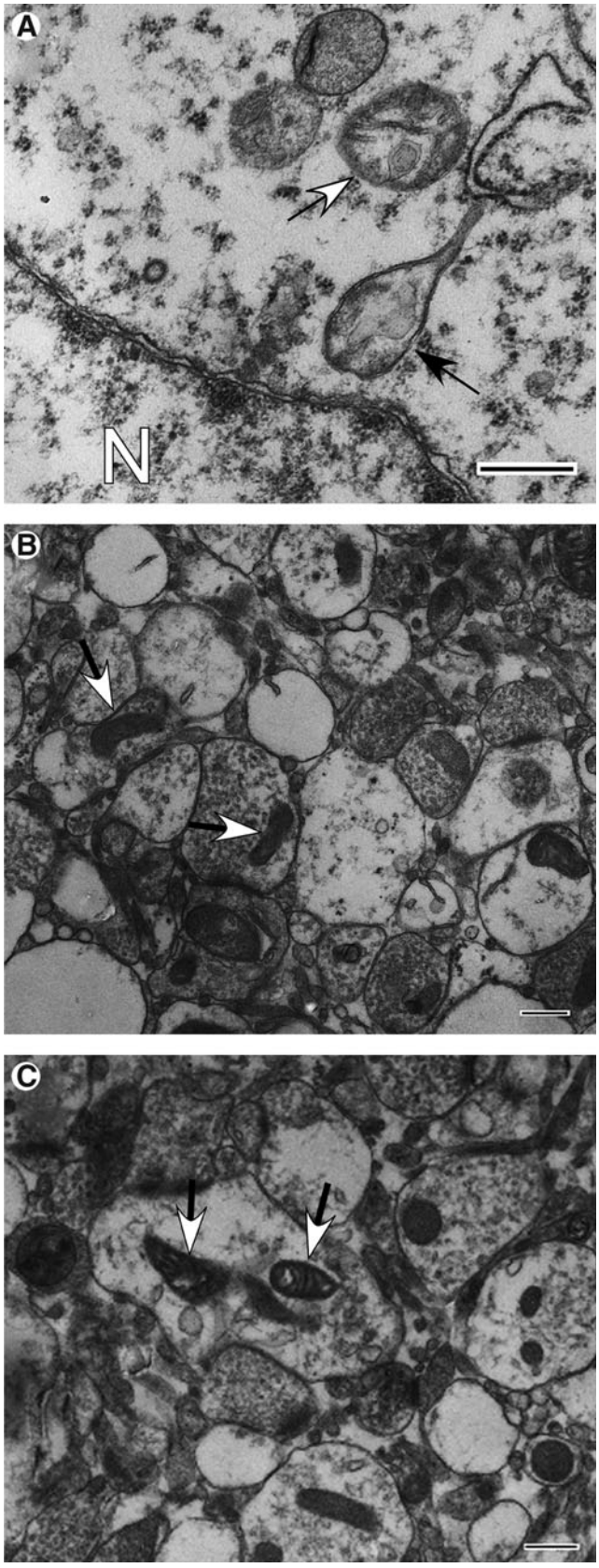

FIG. 12. Ultrastructural pathology of injured cortex, Far zone (Case #12) at intermediate injury phase (between 1 and 3 days post-injury). (**A**) Perinuclear area showing moderate edema of cytoplasm, and mitochondrial profiles showing degenerative changes of cristate structure and clear expanded matrix (arrows). A profile shows undergoing thread-like extension of inner and outer membranes suggesting an arrested thread-grain transition (black arrow). N, nucleus. (**B**) Area of neuropil showing widespread edematous expansion of cell processes and synaptic terminals as well as variation in mitochondrial size, shape, and matrix density. Arrows show normal reactive mitochondria with condensed matrix. (**C**) Area of neuropil showing moderate swelling of cell processes. Note cell process with edematous swelling and containing condensed twisted mitochondria (arrows). Scale bars equal 500 nm.

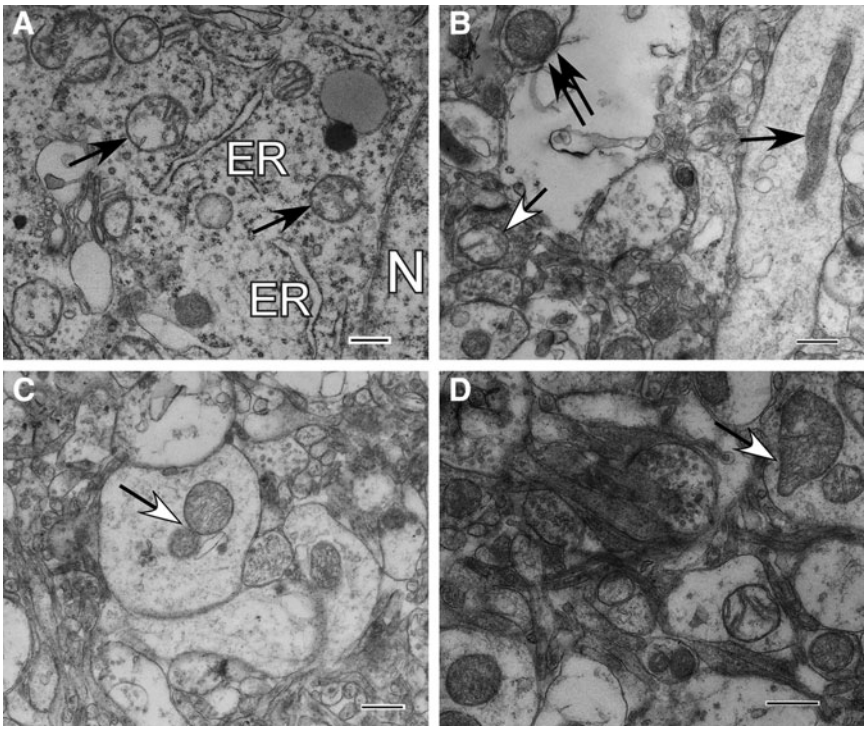

FIG. 13. Ultrastructural pathology of injured cortex, Penumbra zone (Case #12) at intermediate injury phase (between 1 and 3 days post-injury). (**A**) Neuronal cell with good preservation of nucleus (N), cytoplasm, and even distribution of organelles. Endoplasmic reticulum (ER) cisternae are in a normal configuration. Mitochondria, however, exhibit abnormally spherical profiles with clear matrix space and disruption of cristate architecture (black arrows). (**B**) Neuropil with numerous swollen cell processes and a wide range of mitochondrial profiles including spherical mitochondria with normal density matrix and apparent cristate proliferation (double black arrows) or with clear matrix space and disruption of cristate architecture (arrow with white head). A filamentous orthodox mitochondrion (black arrow) is also seen. (**C**) Swollen cell processes with advanced cytoskeletal fragmentation and contiguous spherical mitochondrial profiles suggestive of budding or fission (arrow). (**D**) Neuropil with frequent swollen processes showing mitochondrial changes. Note the teardrop-shaped mitochondrial profile suggestive of a late thread-grain transition (arrow). All scale bars are 500 nm.

(19% ± 2.1 vs. 5.3% ± 1.3) ($p \leq 0.0001$) when compared with control tissue (Fig. 11).

Discussion

The purpose of this study was to characterize the ultrastructure of neuronal mitochondria present in the Near, Far, and Penumbra focal injury areas within the cortex of patients with TBI and to compare these with the mitochondrial ultrastructure observed with control human cerebral cortex. We also assessed whether different post-injury intervals affected changes in mitochondrial morphotypes seen after TBI. Because of the diversity of ages, sex, GCS scores, and time after injury when tissue was collected, this preliminary work cannot be considered to represent the entire spectrum of mitochondrial ultrastructural phenotypes and pathologies. Further, an inherent limitation of conventional transmission electron microscopy used in this work is that it shows a random 2D projection image of the mitochondria but does not display overall mitochondrial shape. Further three-dimensional EM reconstruction of the mitochondria is necessary to exclude the limitation.[39] The value of this work is in bringing to light a pattern of related changes and in providing a framework for evaluation of the significance of future cerebral cortical cytoarchitectural and cytochemical observations on these and other study subjects.

The tissues in these studies were fixed by immersion in a 4% formaldehyde-1% glutaraldehyde combination primary fixative. Because both penetration of fixative into the brain tissue fragment and ultrastructural changes related to ischemia are time dependent, one must factor these parameters into the interpretation of our findings. In the ''*in vitro* necrosis'' study,[40] using 2% osmium tetroxide only or alternatively, 6% glutaraldehyde only as the primary fixative, progressive mitochondrial ultrastructural alterations occurred at finite time intervals. Only loss of their usual matrix granules was observed after 15 min. After 30 minutes, mitochondria were structurally unremarkable except for some enlargement of the matrix compartment and some loss of matrix density. Only after 1 h were there recognizable irregularities of the contour of the outer membrane and membrane-associated flocculent densities.

Our studies used 4% formaldehyde as a primary fixative. Because formaldehyde penetrates and complexes proteins at a 5 to 10 times faster rate than either glutaraldehyde alone or osmium tetroxide alone[41] and because immersion of the tissues in this study occurred within 10 min of separation from the patient's vascular circulation, it is unlikely that this amount of ischemia resulted in any of the structural changes beyond those also apparent abnormalities noted in our control tissue. On the other hand, because there is a very dynamic association between microtubules and mitochondrial shape and trafficking between the nucleus and synaptic junctions, *in vivo* sectioning injury of an axon may result in changes in their distribution and structure in both the control and TBI cases. It is also possible that the anesthetics used during either the TBI tissue resections or the epilepsy lobectomy could influence mitochondrial ultrastructure; however, such effects appear restricted to prolonged exposure of the immature brain to anesthesia.[42]

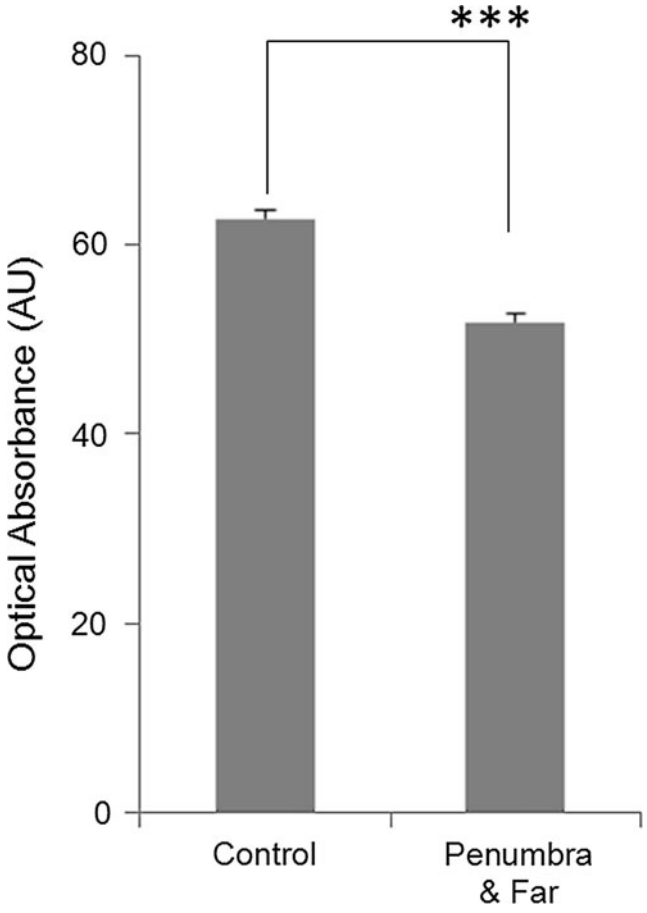

FIG. 14. Optical Absorbance of normal mitochondria exhibiting an orthodox conformation present in human traumatic brain injury (TBI) (Fig. 13B (black arrow)) and control cortex (Fig. 7A, arrows). Absorbance units (AU) obtained from the cytoplasm present immediately adjacent to mitochondria were defined as background absorbance and subtracted from the AU recorded for entire mitochondria. $n = 390$ for control tissue; $n = 78$ for TBI tissue, using both Far and Penumbra zones. ***$p \leq 0.001$.

We draw the following general conclusions from our analyses of mitochondrial ultrastructural changes after human TBI: first, cerebral cortical mitochondria undergo many diverse and striking morphological changes apparent in tissue samples surgically resected and rapidly placed in fixative. These changes are most wide-ranging at the intermediate post-injury time of 38 h (plus or minus a few hours) within the first week post-injury and when GCS scores are not severely low. When GCS scores are as low as 3 or 5, the mitochondrial changes are not so varied. Even at the early post-injury phase, the mitochondria exhibit primarily end-stage degenerating profiles, when GCS scores are low. When GCS scores are moderate or high, Far and Penumbral zones exhibit primarily normal and normal reactive mitochondrial categories at early post-injury phase. Rare reactive/degenerative mitochondria display predominantly thread-grain-transition profiles. At late stage within the first week post-injury, mitochondrial ultrastructural changes are occasional to rare. Mitochondria exhibit primarily reactive/degenerating profiles in Far and Penumbra zones and end-stage degenerating profiles in Near zone. These findings support our hypothesis that changes in mitochondrial ultrastructure reflect overall severity of TBI, that they vary from one post-injury interval to another, and that levels of irreversible (end-stage degenerating) and reversible (normal reactive) mitochondrial changes reflect regional levels of brain injury severity. We speculate that if TBI is severe, the transformation of mitochondrial morphology from normal to irreversibly damaged occurs more rapidly than when TBI is mild or moderate.

Second, quantitative analysis derived from our representative case reveals statistically significant differences in four mitochondrial morphologic categories both between the three contiguous cortical injury zones and between these zones and control cerebral cortex tissue obtained during an epilepsy lobectomy.

Third, changes in morphological categories in the Near, Far, and Penumbral injury areas are associated with additional changes in other markers of neuronal pathology—e.g., cell membrane disruption, cytoplasmic edema, and nuclear structural alterations, which also vary among these zones. Previously, it was found that different cortical contusion zones ranging from the injury center, through its periphery, to the surrounding penumbra, display specific pathological characteristics, e.g., blood flow and oxygenation, in both human and experimental TBI.[43–47] Considering the dependence of mitochondrial structure and energetics on the availability of biofuel and oxygen, the differences in mitochondrial morphology among these zones is consistent with these gradients.

The mitochondrial phenotypes consistently observed in our 22 TBI cases include: (A) profiles associated with conformational changes typically associated with different rates of aerobic energy metabolism; (B) morphodynamic alterations, including division, thread-grain transition, budding, outer membrane blebbing, loop and donut-shaped (toroidal) formations; (C) mitochondrial accumulation in bulbous enlargements along dendrites and axons; (D) intramitochondrial accumulation of dark precipitates and diffuse granules; (E) appearance of mitochondrial forms involving low and high amplitude swelling; and (F) mitochondrial authophagy.

Based on the structural status and integrity of the matrix, cristae, and outer and inner membranes, mitochondria were grouped into four categories: normal, normal reactive, reactive degenerating, and end-stage degenerating phenotypes. Many additional sub-categories were also identified. A tissue sample of a representative case acquired at 38 h post-injury was selected for detailed mitochondrial quantification. According to our unpublished results, at approximately 38 h post-injury, there is a peak of cellular edematous changes within the first week post-injury. This case provided all three injury zones for comparative analysis between changes in mitochondrial morphology and different regional levels of brain injury severity.

In the central injury zone (Near), there is widespread cellular fragmentation with end-stage degenerating mitochondria as the primary mitochondrial phenotype. Edematous loose necrotic material, marked dilatation of vascular spaces, vascular stasis, and interstitial hemorrhage are characteristic for this zone. The Far and Penumbra zones exhibit more normal-appearing cellular morphology and numerous normal reactive mitochondria. The Far zone, however, appears less well preserved than the Penumbra zone and is characterized by intra- and extracellular edema, focal perivascular hemorrhage, and occasional reactive/degenerative changes in cellular organelles. The number of end-stage degenerating mitochondria is significantly higher in the Far zone than in both the Penumbra zone and control tissue. Although the Penumbra zone is better preserved than the Near and Far zones, evidence for intracellular swelling and changes in cellular organelles are present.

In contrast to control tissue, the Penumbra zone exhibits significantly fewer normal ''orthodox'' mitochondria and a larger number of reactive/degenerating mitochondria. In comparison with mitochondria present in control tissues, orthodox mitochondria from TBI tissues exhibit a significant reduction in optical density,

suggesting a dilution and/or loss of matrix contents. This finding also suggests that this relatively electron translucent, orthodox-like mitochondrial profile in TBI tissue could represent an early stage during mitochondrial swelling.[38]

Mitochondria grouped to the normal category are similar in appearance to the conformations termed orthodox, which is often associated with relatively low, basal respiration.[26–28] These mitochondria are elongate and tubular or ovoid/spherical with moderately dense matrix and well preserved cristate and membrane structures. Normal reactive mitochondria frequently display morphologies consistent with a ''condensed'' conformation, which is typically associated with rapid respiration in response to physiologically stimulated oxidative phosphorylation.[26–28]

Far and Penumbral zones exhibit significantly more normal reactive mitochondria when compared with control tissue. Elevated aerobic energy metabolism has been demonstrated in the cortical Penumbral zone of TBI patients,[47] which is consistent with increased mitochondria displaying a condensed conformation in this zone. Increased mitochondrial biogenesis has also been reported in neurons of the cortical infarct border zone after hypoxic-ischemic brain injury.[48] Some of the normal reactive mitochondria display transformation of the matrix to a dense ''twisted'' conformation. This morphotype represents an intermediate, reversible stage of mitochondrial swelling.[38] The most striking mitochondrial morphological subtype present in the normal reactive category is donut-shaped mitochondria and their loop-like intermediates. Similar toroidal mitochondria have been observed after hypoxia-reoxygenation and may be caused by dissociation of mitochondria from microtubules and anomalous mitochondrial fusion.[6]

The reactive degenerating mitochondrial category is represented mainly by mitochondria undergoing various fission processes. These processes include thread-grain transition and appearance of spheroidal mitochondria in the absence or presence of dense inclusions. Other fission-related morphologies include mitochondrial division and mitochondrial membrane blebbing. Evidence obtained from *in vitro* studies suggest that the thread-grain transition is mediated by a dynamin-related protein 1, precedes cell death, and is accompanied by ultrastructural alterations, autophagy, loss of cellular ATP, and oxidative stress.[24,33,49] It is also possible that some of the fission-related morphologies observed after TBI represent adaptive mitochondrial biogenesis in response to metabolic stress.

There is massive mitochondrial accumulation in varicosities of neuronal processes within the first week post-injury that may focally increase the production of reactive oxygen species and/or pro-apoptotic proteins by the mitochondria. The analogous massive mitochondrial accumulation was previously demonstrated both in human TBI axons[50] and in rodent dendrites and axons after cerebral ischemia.[51] The end-stage degenerating mitochondrial category is typified by spherical fission products represented mainly by swollen mitochondria with electron-dense diffusely granular matrix and/or matrix dense inclusions. These mitochondrial profiles are most and least abundant in the Near zone and Penumbra zone, respectively. Similar patterns of structural alterations to neuronal mitochondria have been shown to occur during reperfusion after cerebral ischemia.[52]

Mitochondrial flocculent densities can precede matrix granulation and may be a reliable indicator of irreversible mitochondrial injury.[36] Although the exact pathophysiology of these mitochondrial structural alterations is unknown, cellular calcium dysregulation may be responsible.[53–56] When intramitochondrial calcium reaches a critical level, the mitochondrial permeability transition pore opens, leading to mitochondrial depolarization, loss of mitochondrial metabolites, osmotic swelling, and necrotic cell death.[53–56] Other calcium-dependent activities that could contribute to end-stage mitochondrial degeneration include calpain-mediated proteolysis and phospholipase-mediated membrane lipid hydrolysis.

Based on our observations and evidence from experimental models, we propose that the mitochondrial structural alterations that occur in human cortical TBI tissue are associated with both perturbations in mitochondrial dynamics and with osmotic swelling associated with mitochondrial permeability transition (MPT) pore openings.[2,57–60] It has now been demonstrated that inhibition of the MPT after TBI is a viable neuroprotective approach[61–63] and can improve the favorable outcomes of severe TBI patients.[64,65] The several interrelated mitochondrial dynamic processes, such as fusion, fission, anterograde and retrograde transport in axons, turnover, and interaction with cytoskeleton and other organelles, form a complex interacting network that governs mitochondrial function and thereby cellular integrity.[4] Pharmacologic approaches toward minimizing abnormal alterations in mitochondrial dynamics warrant exploration and might exert neuroprotection beyond what has been observed with inhibitors of the mitochondrial permeability transition that help maintain mitochondrial and cellular integrity.[66]

Our data suggest that TBI therapeutic interventions might target mitochondria in Far and Penumbral zones to protect and preserve potentially viable cortical tissue. In contrast to Near zone, these zones appear to exhibit high levels of reversibly altered mitochondria within the first few days to 1 week post-injury, depending on the severity (GCS) of the injury.

Acknowledgments

The authors express a special thanks and appreciation to Dr. Ru-Ching Hsia, Associate Professor, Director of Core Imaging Facility at University of Maryland Dental School, for her expert technical advice and also for making available the electron microscope used in this study, and Ms. Maritza Patton (Department of Pathology at University of Maryland School of Medicine) for her help with preparation of tissue sections for electron microscopy.

This work was supported by NIH grants T32 GM075776 and P01 HD16596 and a grant from Paragon Bioservices, Inc.

Author Disclosure Statement

No competing financial interests exist.

References

1. Fiskum, G. (2000). Mitochondrial participation in ischemic and traumatic neural cell death. J. Neurotrauma 17, 843–855.
2. Lifshitz, J., Sullivan, P.G., Hovda, D.A., Wieloch, T., and McIntosh, T.K. (2004). Mitochondrial damage and dysfunction in traumatic brain injury. Mitochondrion 4, 705–713.
3. Okonkwo, D.O., and Povlishock, J.T. (1999). An intrathecal bolus of cyclosporin A before injury preserves mitochondrial integrity and attenuates axonal disruption in traumatic brain injury. J. Cereb. Blood Flow Metab. 19, 443–451.
4. Bereiter-Hahn, J., and Jendrach, M. (2010). Mitochondrial dynamics. Int. Rev. Cell Mol. Biol. 284, 1–65.
5. Garrido, N., Griparic, L., Jokitalo, E., Wartiovaara, J., van der Bliek, A.M., and Spelbrink, J.N. (2003). Composition and dynamics of human mitochondrial nucleoids. Mol. Biol. Cell. 14, 1583–1596.
6. Liu, X., and Hajnoczky, G. (2011). Altered fusion dynamics underlie unique morphological changes in mitochondria during hypoxia-reoxygenation stress. Cell Death Differ. 18, 1561–1572.
7. Lyamzaev, K.G., Nepryakhina, O.K., Saprunova, V.B., Bakeeva, L.E., Pletjushkina, O.Y., Chernyak, B.V., and Skulachev, V.P. (2008). Novel mechanism of elimination of malfunctioning mitochondria (mitoptosis): formation of mitoptotic bodies and extrusion of mitochondrial material from the cell. Biochim. Biophys. Acta 1777, 817–825.

8. Mannella, C.A. (2006). The relevance of mitochondrial membrane topology to mitochondrial function. Biochim. Biophys. Acta 1762, 140–147.
9. Zick, M., Rabl, R., and Reichert, A.S. (2009). Cristae formation-linking ultrastructure and function of mitochondria. Biochim. Biophys. Acta 1793, 5–19.
10. Jahani-Asl, A., Pilon-Larose, K., Xu, W., MacLaurin, J.G., Park, D.S., McBride, H.M., and Slack, R.S. (2011). The mitochondrial inner membrane GTPase, optic atrophy 1 (Opa1), restores mitochondrial morphology and promotes neuronal survival following excitotoxicity. J. Biol. Chem. 286, 4772–4782.
11. Chen, H., and Chan, D.C. (2009). Mitochondrial dynamics—fusion, fission, movement, and mitophagy—in neurodegenerative diseases. Hum. Mol. Genet. 18, R169–R176.
12. Gunawardena, S., and Goldstein, L.S. (2004). Cargo-carrying motor vehicles on the neuronal highway: transport pathways and neurodegenerative disease. J. Neurobiol. 58, 258–271.
13. Liesa, M., Palacin, M., and Zorzano, A. (2009). Mitochondrial dynamics in mammalian health and disease. Physiol. Rev. 89, 799–845.
14. Morganti-Kossmann, M.C., Yan, E., and Bye, N. (2010). Animal models of traumatic brain injury: is there an optimal model to reproduce human brain injury in the laboratory? Injury 41, Suppl 1, S10–S13.
15. Vink, R., and Nimmo, A.J. (2009). Multifunctional drugs for head injury. Neurotherapeutics 6, 28–42.
16. Castejon, O.J., and De Castejon, H.V. (2004). Structural patterns of injured mitochondria in human oedematous
17. Balan, I.S., Kristian, T., Liu, C., Saladino, A.J., and Hu, B. (2012). Morphological assessments of global cerebral ischemia: Electron microscopy, in: *Animal Models of Acute Neurological Injuries II.* J. Chen, X.-M. Xu, Z.C. Xu, and J.H. Zhang (eds). Humana Press: New York, pps. 29–46.
18. Cragg, B.G. (1976) Ultrastructural features of human cerebral cortex. J. Anat. 121, 331–362.
19. Harris, K.M. (2008). Diversity in synapse structure and composition, in: *Structural and Functional Organization of the Synapse.* J.W. Hell, and M.D. Ehlers (eds). Springer: New York, pps. 1–21.
20. Mishchenko, Y., Hu, T., Spacek, J., Mendenhall, J., Harris, K.M., and Chklovskii, D.B. (2010) Ultrastructural analysis of hippocampal neuropil from the connectomics perspective. Neuron 67, 1009–1020.
21. Ong, W.Y., and Garey, L.J. (1991). Ultrastructural characteristics of human adult and infant cerebral cortical neurons. J. Anat. 175, 79–104.
22. Peters A., Palay S.L., and Webster, H. deF (1991). *The Fine Structure of the Nervous System.* Oxford University Press: New York.
23. Balan, I.S., Fiskum, G., and Kristian, T. (2010). Visualization and quantification of NAD(H) in brain sections by a novel histo-enzymatic nitrotetrazolium blue staining technique. Brain Res. 1316, 112–119.
24. Barsoum, M.J., Yuan, H., Gerencser, A.A., Liot, G., Kushnareva, Y., Gräber, S., Kovacs, I., Lee, W.D., Waggoner, J., Cui, J., White, A.D., Bossy, B., Martinou, J.C., Youle, R.J., Lipton, S.A., Ellisman, M.H., Perkins, G.A., and Bossy-Wetzel, E. (2006). Nitric oxide-induced mitochondrial fission is regulated by dynamin-related GTPases in neurons. EMBO J. 25, 3900–3911.
25. Benani, A., Barquissau, V., Carneiro, L., Salin, B., Colombani, A.L., Leloup, C., Casteilla, L., Rigoulet, M., and Penicaud, L. (2009). Method for functional study of mitochondria in rat hypothalamus. J. Neurosci. Methods 178, 301–307.
26. Hackenbrock, C.R. (1966). Ultrastructural bases for metabolically linked mechanical activity in mitochondria. I. Reversible ultrastructural changes with change in metabolic steady state in isolated liver mitochondria. J. Cell Biol. 30, 269–297.
27. Hackenbrock, C.R. (1968). Ultrastructural bases for metabolically linked mechanical activity in mitochondria. II. Electron transport-linked ultrastructural transformations in mitochondria. J. Cell Biol. 37, 345–369.
28. Hackenbrock, C.R., Rehn, T.G., Weinbach, E.C., and Lemasters, J.J. (1971). Oxidative phosphorylation and ultrastructural transformation in mitochondria in the intact ascites tumor cell. J. Cell Biol. 51, 123–137.
29. Lai, Y., Chen, Y., Watkins, S.C., Nathaniel, P.D., Guo, F., Kochanek, P.M., Jenkins, L.W., Szabó, C., and Clark, R.S. (2008). Identification of poly-ADP-ribosylated mitochondrial proteins after traumatic brain injury. J. Neurochem. 104, 1700–1711.
30. Singh, I.N., Sullivan, P.G., Deng, Y., Mbye, L.H., and Hall, E.D. (2006). Time course of post-traumatic mitochondrial oxidative damage and dysfunction in a mouse model of focal traumatic brain injury: implications for neuroprotective therapy. J. Cereb. Blood Flow Metab. 26, 1407–1418.
31. Sloper, J.J., Hiorns, R.W., and Powell, T.P. (1979). A qualitative and quantitative electron microscopic study of the neurons in the primate motor and somatic sensory cortices. Philos. Trans. R. Soc. Lond. B. Biol. Sci. 285, 141–171.
32. Packer, L. (1970). Relation of structure to energy coupling in rat liver mitochondria. Fed. Proc. 29, 1533–1540.
33. Skulachev, V.P., Bakeeva, L.E., Chernyak, B.V., Domnina, L.V., Minin, A.A., Pletjushkina, O.Y., Saprunova, V.B., Skulachev, I.V., Tsyplenkova, V.G., Vasiliev, J.M., Yaguzhinsky, L.S., and Zorov, D.B. (2004). Thread-grain transition of mitochondrial reticulum as a step of mitoptosis and apoptosis. Mol. Cell Biochem. 256–257, 341–358.
34. Neuspiel, M., Schauss, A.C., Braschi, E., Zunino, R., Rippstein, P., Rachubinski, R.A., Andrade-Navarro, M.A., and McBride, H.M. (2008). Cargo-selected transport from the mitochondria to peroxisomes is mediated by vesicular carriers. Curr. Biol. 18, 102–108.
35. Greenawalt, J.W., Rossi, C.S., and Lehninger, A.L. (1964). Effect of active accumulation of calcium and phosphate ions on the structure of rat liver mitochondria. J. Cell Biol. 23, 21–38.
36. Trump, B.F., Mergner, W.J., Kahng, M.W., and Salandino, A.J. (1976). Studies on the subcellular pathophysiology of ischemia. Circulation 53, Suppl 3, I17–I26.
37. Liu, C., Gao, Y., Barrett, J., and Hu, B. (2010). Autophagy and protein aggregation after brain ischemia. J. Neurochem. 115, 68–78.
38. Myron, D.R., and Connelly, J.L. (1971). The morphology of the swelling process in rat liver mitochondria. J. Cell Biol. 48, 291–302.
39. Popov, V., Medvedev, N.I., Davies, H.A., and Stewart, M.G. (2005). Mitochondria form a filamentous reticular network in hippocampal dendrites but are present as discrete bodies in axons: a three-dimensional ultrastructural study. J. Comp. Neurol. 492, 50–65.
40. Trump, B.F., Goldblatt, P.J., and Stowell, R.E. (1965). Studies on necrosis of mouse liver in vitro. Ultrastructural alterations in the mitochondria of hepatic parenchymal cells. Lab. Invest. 14, 343–371.
41. Johannessen, J.V. (1978). *Electron Microscopy in Human Medicine: Instrumentation and techniques*. J.V. Johannessen (ed). McGraw-Hill: New York, pps. 1–348.
42. Sanchez, V., Feinstein, S.D., Lunardi, N., Joksovic, P.M., Boscolo, A., Todorovic, S.M, and Jevtovic-Todorovic, V. (2011) General anesthesia causes long-term impairment of mitochondrial morphogenesis and synaptic transmission in developing rat brain. Anesthesiology 115, 992–1002.
43. Immonen, R., Heikkinen, T., Tähtivaara, L., Nurmi, A., Stenius, T.K., Puoliväli, J., Tuinstra, T., Phinney, A.L., Van Vliet, B., Yrjänheikki, J., and Gröhn, O. (2010). Cerebral blood volume alterations in the perilesional areas in the rat brain after traumatic brain injury—comparison with behavioral outcome. J. Cereb. Blood Flow Metab. 30, 1318–1328.
44. Taiushev, K.G., and Shustova, T.I. (1999). [Histologic foundations for evaluation of the crushed wound of the cerebrum in the clinical course of cranio-cerebral trauma as an intracranial extensive process]. (Rus) Morfologiia 116, 7–11.
45. Taiushev, K.G., Zotov, IuV., Kaganovskaia, E.A., Kasumov, R.D., and Shustova, T.I. (1990). [Changes in human cerebral cortex in various areas of concussion in severe cranio-cerebral injury.] (Rus) Arkh. Anat. Gistol. Embriol. 99, 26–33.
46. Thomale, U.W., Griebenow, M., Mautes, A., Beyer, T.F., Dohse, N.K., Stroop, R., Sakowitz, O.W., Unterberg, A.W., and Stover, J.F. (2007). Heterogeneous regional and temporal energetic impairment following controlled cortical impact injury in rats. Neurol. Res. 29, 594–603.
47. Ugriumov, V.M., Zotov, IuV., Tigliev, G.S., and Kondakov, E.N. (1977). [Several pathophysiologic grounds for radical removal of contusion foci from the cerebral hemispheres]. (Rus) Zh. Vopr. Neirokhir. Im. N. N. Burdenko, 3–7.
48. Yin, W., Signore, A.P., Iwai, M., Cao, G., Gao, Y., and Chen, J. (2008). Rapidly increased neuronal mitochondrial biogenesis after hypoxic-ischemic brain injury. Stroke 39, 3057–3063.
49. Frank, S., Gaume, B., Bergmann-Leitner, E.S., Leitner, W.W., Robert, E.G., Catez, F., Smith, C.L., and Youle, R.J. (2001). The role of dynamin-related protein 1, a mediator of mitochondrial fission, in apoptosis. Dev. Cell 1, 515–525.

50. Christman, C.W., Grady M.S., Walker, S.A., Holloway, K.L, and Povlishock, J.T. (1994). Ultrastructural studies of diffuse axonal injury in humans. J. Neurotrauma 11, 173–186.
51. Colbourne, F., Sutherland, G.R., and Auer, R.N. (1999). Electron microscopic evidence against apoptosis as the mechanism of neuronal death in global ischemia. J. Neurosci. 19, 4200–4210.
52. Solenski, N.J., diPierro, C.G., Trimmer, P.A., Kwan, A.L., and Helms, G.A. (2002). Ultrastructural changes of neuronal mitochondria after transient and permanent cerebral ischemia. Stroke 33, 816–824.
53. Ahn, E.S., Robertson, C.L., Vereczki, V., Hoffman, G.E., and Fiskum, G. (2008). Normoxic ventilatory resuscitation following controlled cortical impact reduces peroxynitrite-mediated protein nitration in the hippocampus. J. Neurosurg. 108, 124–131.
54. Kristian, T., and Siesjö, B.K. (1996). Calcium-related damage in ischemia. Life Sci. 59, 357–367.
55. Lifshitz, J., Friberg, H., Neumar, R.W., Raghupathi, R., Welsh, F.A., Janmey, P., Saatman, K.E., Wieloch, T., Grady, M.S., and McIntosh, T.K. (2003). Structural and functional damage sustained by mitochondria after traumatic brain injury in the rat: evidence for differentially sensitive populations in the cortex and hippocampus. J. Cereb. Blood Flow Metab. 23, 219–231.
56. Starkov, A.A., Chinopoulos, C., and Fiskum, G. (2004). Mitochondrial calcium and oxidative stress as mediators of ischemic brain injury. Cell Calcium 36, 257–264.
57. Büki, A., Okonkwo, D.O., Wang, K.K., and Povlishock, J.T. (2000). Cytochrome c release and caspase activation in traumatic axonal injury. J. Neurosci. 20, 2825–2834.
58. Kroemer, G., and Reed, J.C. (2000). Mitochondrial control of cell death. Nat. Med. 6, 513–519.
59. Mazzeo, A.T., Beat, A., Singh, A., and Bullock, M.R. (2009). The role of mitochondrial transition pore, and its modulation, in traumatic brain injury and delayed neurodegeneration after TBI. Exp. Neurol. 218, 363–370.
60. Sullivan, P.G., Rabchevsky, A.G., Waldmeier, P.C., and Springer, J.E. (2005). Mitochondrial permeability transition in CNS trauma: cause or effect of neuronal cell death? J. Neurosci. Res. 79, 231–239.
61. Büki, A., Okonkwo, D.O., and Povlishock, J.T. (1999). Postinjury cyclosporin A administration limits axonal damage and disconnection in traumatic brain injury. J. Neurotrauma 16, 511–521.
62. Cook, A.M., Whitlow, J., Hatton, J., and Young, B. (2009). Cyclosporine A for neuroprotection: establishing dosing guidelines for safe and effective use. Expert Opin. Drug Saf. 8, 411–419.
63. Sullivan, P.G., Sebastian, A.H., and Hall, E.D. (2011). Therapeutic window analysis of the neuroprotective effects of cyclosporine A after traumatic brain injury. J. Neurotrauma 28, 311–318.
64. Hatton, J., Rosbolt, B., Empey, P., Kryscio, R., and Young, B. (2008). Dosing and safety of cyclosporine in patients with severe brain injury. J. Neurosurg. 109, 699–707.
65. Mazzeo, A.T., Brophy, G.M., Gilman, C.B., Alves, O.L., Robles, J.R., Hayes, R.L., Povlishock, J.T., and Bullock, M.R. (2009). Safety and tolerability of cyclosporin a in severe traumatic brain injury patients: results from a prospective randomized trial. J. Neurotrauma 26, 2195–2206.
66. Perez-Pinzon, M.A., Stetler, R.A., and Fiskum, G. (2012). Novel mitochondrial targets for neuroprotection. J. Cereb. Blood Flow Metab. 32, 1362–1376.

Address correspondence to:
Gary Fiskum, PhD
Department of Anesthesiology
University of Maryland School of Medicine
685 W. Baltimore Street MSTF 5.34
Baltimore, MD 21201

E-mail: gfiskum@anes.umm.edu